CHEMISTRY OF MATERIALS

Article

pubs.acs.org/cm

Molten Salt Assisted Self Assembly (MASA): Synthesis of Mesoporous Metal Titanate ($CoTiO_3$, $MnTiO_3$, and $Li_4Ti_5O_{12}$) Thin Films and Monoliths

Civan Avcı,[†] Aykut Aydın,[†] Zeynep Tuna,[†] Zelal Yavuz,[†] Yusuke Yamauchi,[‡,§,∥] Norihiro Suzuki,[⊥] and Ömer Dag*[,†]

[†]Department of Chemistry, Bilkent University, 06800 Ankara, Ankara, Turkey

[‡]World Premier International (WPI) Research Center for Materials Nanoarchitectonics (MANA), National Institute for Materials Science (NIMS), 1-1 Namiki, Tsukuba, Ibaraki 305-0044, Japan

[§]Faculty of Science and Engineering, Waseda University, 3-4-1 Okubo, Shinjuku, Tokyo 169-8555, Japan

[∥]Institute for Superconducting and Electronic Materials (SEM), Australian Institute for Innovative Materials, University of Wollongong, North Wollongong, NSW 2500, Australia

[⊥]International Center for Young Scientists (ICYS) National Institute for Materials Science (NIMS) 1-2-1 Sengen, Tsukuba, Ibaraki 305-0047, Japan

Supporting Information

ABSTRACT: Mesoporous metal titanates are very important class of materials for clean energy applications, specifically transition metal titanates and lithium titanates. The molten salt assisted self-assembly (MASA) process offers a new synthetic route to produce mesoporous metal titanate thin films. The process is conducted as follows: first a clear solution that contains two solvents (namely the hydrated salt $(Co(NO_3)_2 \cdot 6H_2O$ or $Mn(NO_3)_2 \cdot 6H_2O$, or $LiNO_3 \cdot xH_2O$, and ethanol), two surfactants (cethyltrimethylammonium bromide, CTAB, and 10-lauryl ether, $C_{12}EO_{10}$), an acid and titanium source (titanium tetrabutoxide, TTB) is prepared and then spin or spray coated over a substrate to form a thin or thick lyotropic liquid crystalline (LLC) film, respectively. Finally, the films are converted into transparent spongy mesoporous metal titanates by a fast calcination step. Three mesoporous metal titanates (namely, $CoTiO_3$, $MnTiO_3$, and $Li_4Ti_5O_{12}$) have been successfully synthesized and structurally/thermally characterized using microscopy, spectroscopy, diffraction, and thermal techniques. The mesoporous cobalt and manganese titanates are stable up to 500 °C and collapse at around 550 °C into nanocrystalline Co_3O_4−TiO_2 and Mn_2O_3−TiO_2; however, lithium titanate is stable up to 550 °C and crystalline even at 350 °C. The crystallinity and pore size of these titanates can be adjusted by simply controlling the annealing and/or calcination temperatures.

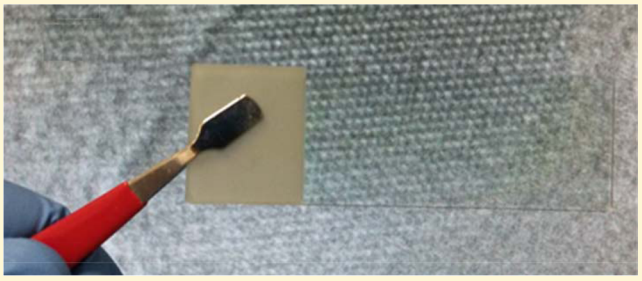

INTRODUCTION

The melting point of metal salts can be reduced significantly in a confined space - known as the confinement effect - such that they may act as solvents in a self-assembly process.[1] Organizing surfactants into lyotropic liquid crystalline (LLC) mesophases by using molten salts can be beneficial in the production of new materials for clean energy applications.[2,3] Recently, we have demonstrated that the molten phase of salts can be used as a solvent in the synthesis of mesoporus metal oxide modified silica[2] as well as titania.[3] This process was introduced as molten salt assisted self-assembly (MASA).[2,3] The MASA is a useful process in producing materials that are difficult to produce using known synthesis techniques, and it can be regarded as a new synthetic route. Two solvents and two surfactants are needed in this self-assembly process. The first solvent is volatile and is used to homogenize the mixture of the ingredients to produce a clear solution,[2,3] and the second solvent is a salt, which organizes the mixture into an LLC mesophase upon evaporation of the first one.[3] Simply, a clear solution of a mixture of all the ingredients (salt, surfactants, water (or ethanol), polymerizing agent) can be spin coated over a substrate to form a thin film. Further polymerization of the polymerizing component (silica or titania source) takes place in the self-assembled soft media. The MASA process allows for efficient and homogeneous contact between the polymerizing silica or titania and the salt ions. The spin coated fresh samples are usually stable and remain in their LLC phase for a short time; therefore, they need to be heat treated shortly after coating to convert them into mesoporous thin films. We also need two surfactants in this self-assembly process; one of the

Received: August 16, 2014
Revised: September 26, 2014
Published: September 29, 2014

   dx.doi.org/10.1021/cm503020y | Chem. Mater. 2014, 26, 6050−6057

surfactants is a nonionic surfactant (usually oligo(ethylene oxide) surfactants) that forms the LLC phases of salt-surfactants,[4] and the second surfactant is a charged surfactant that enhances the salt content and further stabilize the salt-surfactant LLC mesophases.[5] By using the MASA route, we have already developed mesoporous silica coated metal oxides (such as CdO and ZnO that can be as thin as 1.6 nm)[2] and metal titanates (such as Zn_2TiO_4 and $CdTiO_3$)[3] that can be effectively converted into sulfides and selenides for various purposes.[3,6] Note also that there are a limited number of works in the literature regarding the synthesis of mesoporous metal titanates[3,7−16] by using soft-templating methods.[17] The synthesis of metal oxides have been recently reviewed by several authors,[17,18] including methods that use ionic liquids as solvents.[19] These materials need to be explored for new clean energy applications. For this reason, effective and easy processes are needed.

Note also that the soft-templating processes of metal titanates are limited to large surfactants (triblock or diblock copolymers) that usually produce mesoporous materials with thicker pore-walls with smaller surface area.[16,17,20] No small surfactant soft-templating method exists for the synthesis of mesoporous metal titanates in the literature.[16] Also note that the metal titanates form at high temperatures (250−350 °C). However, the mesostructure formation is usually a low temperature process (typical room temperature to tens of degree), and it is mostly applicable to metal precursors that can be hydrolyzed and polymerized at low temperatures, like metal alkoxides. Therefore, new approaches are needed to overcome these synthetic issues, where the MASA process[2,3] offers some advantages over the other methods and can be used for the synthesis of some of the metal titanates.

Lithium ions are also very important for applications such as ion conducting gel-electrolytes[21−24] and lithium ion batteries.[16,25−34] The formation of LLC mesophases using lithium salts can also be beneficial in the development of liquid crystalline gel-electrolytes[34] as well as in the development of lithium ion containing mesoporous metal oxides.[16,29−34] Note that many lithium metal oxides have been used as anode or cathode materials in lithium ion batteries.[16,25−34] There are also few investigations regarding the synthesis of these materials as mesoporous powders.[16,29−34] The major motivation, behind these investigations, is to increase the capacitance of these materials for better battery performances. However, investigations of the porous versions of these materials are still limited, and as yet there are still no examples using thin films.[16,29−34] Designing lithium ion conducting solid hosts can be beneficial in the developments of fast ion conductors in various clean energy applications.

In this work, we demonstrate that the MASA is a useful process that can be used to produce mesoporous thin films of $CoTiO_3$, $MnTiO_3$, and $Li_4Ti_5O_{12}$. The films were characterized, and their thermal and structural properties were investigated using PXRD, Raman, FT-IR, and UV−visible absorption spectroscopy, N_2-sorption, SEM, and TEM techniques.

EXPERIMENTAL SECTION

Materials. All the reagents used in this investigation were purchased from Aldrich and used as received.

Preparation of Clear Solutions of the Precursors of $CoTiO_3$ and $MnTiO_3$. Clear solutions of all the ingredients for 4 Co(II) (or 4 Mn(II)) to 4 Ti(IV) were prepared as follows (these ratios are per $C_{12}EO_{10}$): put 291 mg of CTAB and 931 mg of $[Co(H_2O)_6](NO_3)_2$ (or 803 mg of $[Mn(H_2O)_6](NO_3)_2$) in a 25 mL vial, then add 9 mL of ethanol, and stir the mixture on a magnetic stirrer until the mixture becomes clear. Then add 500 mg of $C_{12}EO_{10}$ drop by drop (melt the surfactant first). Stir the mixture for another 5 min. Add 500 mg of 70% HNO_3 and stir for another 5 min to ensure a homogeneous clear solution. Finally, to this clear solution, add 1090 mg of TTB and stir the mixture for an additional 15 min.

For the other compositions, we varied the amount of salts and TTB as follows: for the M(II)/Ti(IV) (M is Co or Mn) ratios of 2/7, 3/7, 4/7, 5/7, 6/7, and 7/7, the amount of TTB was increased to 1908 mg and the $[Co(H_2O)_6](NO_3)_2$ amount was 466, 698, 1164, 1397, and 1629 mg, respectively, and the $[Mn(H_2O)_6](NO_3)_2$ amount was 402, 602, 803, 1004, 1205, and 1405 mg, respectively. The quantities of the surfactants, acid, and ethanol were the same as in the 4/4 M(II)/Ti(IV) samples.

Preparation of Clear Solution of the Precursors of $Li_4Ti_5O_{12}$. Put 291 mg of CTAB, 221 mg of $LiNO_3$, and 9 mL of ethanol in a 25 mL vial and stir it over a magnetic stirrer until the solution is clear. Then add 500 mg of $C_{12}EO_{10}$ and stir the mixture for 5 min. To the above solution 500 mg of 70% HNO_3 was added and stirred for another 5 min. Finally, 1360 mg of TTB was added, and the solution was stirred for another 15 min.

Preparation of $CoTiO_3$, $MnTiO_3$, and $Li_4Ti_5O_{12}$ Thin Films. Put a few drops from each of the above solutions (separately) over a substrate that is already installed on a spin coater and spin the sample at 1500 rpm for 10 s. This produces gel-like thin films. Then insert the films straight into a preheated oven and carry out the calcination for 20 min. Once complete, first cool the oven to 200−300 °C and then remove the samples for analysis. Calcination has been performed at different temperatures between 350 and 600 °C using 50 °C increments.

Preparation of $CoTiO_3$, $MnTiO_3$, and $Li_4Ti_5O_{12}$ Powders by Spray Coating. To produce large quantities of the samples, we also developed a spray coating method. The above clear solutions were separately spray coated over precleaned glass substrates using pressurized dry air until the glass slide was covered. Then the films were immediately inserted into a preheated oven and calcined for 30 min. The calcined samples were removed from the oven after cooling and scraped into a vial. Calcination was carried at a desired temperature, and some samples were calcined at 350 °C and then scraped from the glass slides and annealed at different temperature (at 400, 450, 500, and 550 °C) for 2 h to evaluate the thermal properties of the samples.

Instrumentations. The micro-Raman spectra were recorded on a LabRam confocal Raman microscope with a 300 mm focal length. The spectrometer was equipped with a Ventus LP 532, 50 mW, diode pumped solid-state laser operator at 20 mW, with a polarization ratio of 100:1, a wavelength of 532.1 nm, and a 1024 × 256 element CCD camera. The signal collected was transmitted via a fiber optic cable into a spectrometer with 600 g/mm grating. The Raman spectra were collected by manually placing the probe tip on the desired point of the sample over the glass or silicon wafer. The FTIR spectra were recorded between 400 and 4000 cm^{-1} using a Bruker Tensor 27 model FTIR spectrometer, equipped with a Digi Tect TM DLATGS detector and a resolution of 4.0 cm^{-1}. The spectra were recorded using the samples coated over silicon wafers. The UV−vis absorption spectra were recorded on a Cary 5 UV−vis spectrophotometer using thin films, coated over quartz substrates. The XRD patterns were recorded on a Rigaku Miniflex diffractometer using a high power Cu−Kα source operating at 30 kV/15 mA. The samples were spin coated over microscope slides and measured before and after calcination. The powder samples were packed into glass sample holders, and the PXRD patterns were collected at small (1 to 5°) and wide angles (10 to 80°). The OM images were obtained in transmittance mode on a ZEISS Axio Scope A1 polarizing optical microscope. The SEM images were recorded using Hitachi HD-2000 STEM in SEM mode and ZEISS EVO 40. The high resolution transmittance electron microscope (HRTEM) images were recorded on a JEOL JEM 2100F at an operating voltage of 200 kV. The calcined film samples were scraped and ground in a mortar using ethanol and then dispersed using a

dx.doi.org/10.1021/cm503020y | Chem. Mater. 2014, 26, 6050−6057

sonicator for 10 min. One drop of the dispersed ethanol solution was put on a TEM grid and dried over a hot-plate. The N_2 (77.4 K) sorption measurements were performed with a TriStar 3000 automated gas adsorption analyzer (Micrometrics) in a relative pressure range, P/P_0, from 0.01 to 0.99. To provide high accuracy and precision in the determination of P/P_0, the saturation pressure P_0 was measured over 120 min intervals. The powder samples, which were obtained by scraping approximately 10 glass slides of the spray coated thicker films, were dehydrated under a ($\sim 10^{-2}$ Torr) vacuum for 3 h at 250 °C before measuring in order to remove adsorbed water and volatile species in the pores.

RESULTS AND DISCUSSION

In this work, we have synthesized 3 different mesoporous metal oxide thin films as well as powders using the MASA approach, namely $CoTiO_3$, $MnTiO_3$, and $Li_4Ti_5O_{12}$. Each salt system has been optimized first in the solution phase and then in the gel-phase (fresh spin or spray coated samples) and finally in the solid (after calcination) phase. It is known that the nitrate salts of these metals (Co(II), Mn(II), and Li(I)) form LLC mesophases with nonionic surfactants.[4,35,36] The clear solutions, prepared by dissolving the metal nitrate salts, nitric acid, CTAB, $C_{12}EO_{10}$, and TTB in ethanol, are either spin or spray coated over a substrate to prepare the fresh samples. We have investigated a broad range of metal ion to titanium ratios, but the detailed investigation was limited to 4:4 Co(II):Ti(IV) and Mn(II):Ti(IV) and 4:5 Li(I):Ti(IV) per $C_{12}EO_{10}$, where the mesophase is the most ordered. The freshly prepared thin films and spray coated thicker films were immediately calcined at a desired temperature; the coated samples were directly put into an oven at the calcination temperature and kept at that temperature for 10−30 min. The resulting films are highly transparent and show a sponge-like mesoporous network between 350 and 500 °C, see schematic diagram in Scheme 1.

Scheme 1. Schematic Representations of the Synthesis Step with Increasing Temperature[A]

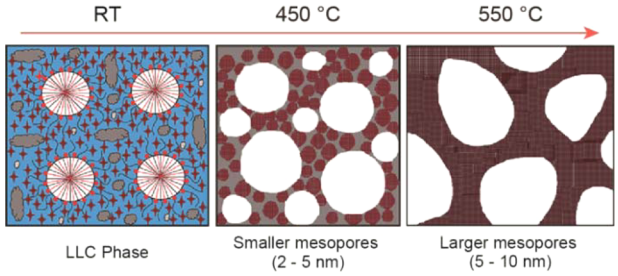

[A]Gray regions are titania species, + salt species, spherical domains are surfactant regions.

Mesoporous $CoTiO_3$ Thin Films and Powders. The MASA process was optimized over a very broad range of $[Co(H_2O)_6](NO_3)_2/C_{12}EO_{10}$ mole ratio keeping all other ingredients constant. We also optimized the amount of acid and the stability of the solution using nitric acid. It was discovered that at low acid end of the mixture (up to 200 mg HNO_3, corresponds to pH of >0.45), the spin coated samples formed worm-like features over the substrate surface, see Figure S1(a and b). These features remain after calcination and are quite mesoporous (pore volume of 0.4 cm^3/g and surface area of 270 m^2/g) with a relatively nonuniform pore size distribution, see Figure S1(c). However, the worm-like features disappeared, and smooth films were obtained when the amount of acid was increased to 500 mg (pH = −0.10), Figure S1(d). We also recorded the small angle XRD patterns of the fresh samples, obtained using various acid amounts in the initial solution. The diffraction line is very broad at low acid concentration and becomes sharper at around 500 mg and above, see Figure S2(a). Even with quantities of nitric acid above 500 mg, the phase is stable and diffracts a sharp line at small angles (see Figure S2(a)), and their calcination produces Co_3O_4 species over the films, Figure S2(b). Figure S3(a and b) shows the SEM image of the samples prepared using 500 and 800 mg of concentrated HNO_3. Both images shows a sponge-like porous structure, but the image of the sample prepared using 800 mg of HNO_3 has small bright spots, which likely originate from impurities, namely the Co_3O_4 nanoparticles. Due to this, we limited our investigation to the samples prepared using 500 mg of acid. All observations and behaviors can be related to the TTB hydrolysis and condensation reaction of the titania species. On the low acid side, the titania formation dominates and controls the assembly; however, in very acidic media the mesostructures leach out some Co(II) salts, which undergo decomposition at higher temperatures to produce Co_3O_4 nanoparticles outside the mesostructure. Therefore, the process requires an optimum amount of acid, which is typically around 500 mg in our reaction conditions and compositions.

We have also investigated the role of salt in the assembly process and varied the cobalt nitrate and TTB amounts in the reaction solution. Figures 1(a) and 1(b) show a set of small angle and wide angle XRD patterns of the freshly prepared films, prepared using various salt contents. The salt to surfactant ratio was varied from 1 to 7, keeping the Ti(IV):$C_{12}EO_{10}$ mole ratio fixed at 7. At low salt contents, the mesophase is stable, but calcination of the samples at 450 °C produced a bulk anatase phase of titania, see Figure 1(c).

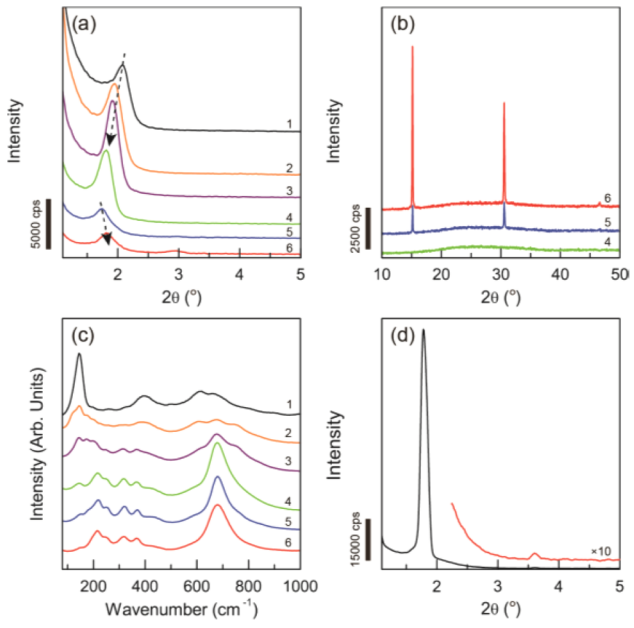

Figure 1. (a) Small angle XRD patterns of the fresh samples with a Co(II):Ti(IV):$C_{12}EO_{10}$ mole ratio of 1:7:1 to 6:7:1 (from top to bottom), (b) wide angle XRD patterns of the fresh samples of 4:7:1, 5:7:1, and 6:7:1 Co(II):Ti)IV):$C_{12}EO_{10}$ mole ratios. (c) Raman spectra calcined samples of set in panel (a). (d) Small angle XRD pattern of the fresh sample of Co(II):Ti(IV):$C_{12}EO_{10}$ of 4:4:1.

dx.doi.org/10.1021/cm503020y | Chem. Mater. 2014, 26, 6050−6057

However, by increasing the salt content of the media the titania formation gradually decreased, and at a salt/surfactant mole ratio above 4, the formation of the anatase phase was completely hindered and the $CoTiO_3$ phase appeared, Figure 1(c). The Raman peaks at 156, 224, 258, 328, 377, 443, and 684 cm^{-1} are due to the ilmenite phase of $CoTiO_3$.[37] The wide angle XRD patterns of the fresh samples display sharp salt related lines at the 5 and 6 Co(II)/$C_{12}EO_{10}$ mole ratios, see Figure 1(b). Additionally, the small angle XRD lines of these samples shift to higher angles, also indicating the leaching of salt species from the mesophase, see Figure 1(a) and 1(b). This is a known phenomenon in a salt-surfactant LLC mesophase, where the unit cell expands to accommodate more salts, but with leaching of the excess salt species, the unit cell shrinks back to low salt values.[5]

We further optimized the synthesis media by playing with the TTB/$C_{12}EO_{10}$ mole ratio and discovered that the optimum TTB/$C_{12}EO_{10}$ mole ratio was also 4. Among all samples investigated, the fresh samples, prepared using a 4:4 Co(II)/Ti(IV) mole ratio, displayed the most intense diffraction line, Figure 1(d). Therefore, this composition was used to further optimize the synthesis method and to characterize the fresh and calcined films. The calcined samples were further characterized using EDS and various modes of TEM, see Figure S4. EDS data and Co and Ti mappings clearly show that the composition is preserved and homogeneous. For the synthesis of large quantities, we also developed a spray coating method. The spray coated samples displayed very similar Raman spectra to that of the thin films before and after calcination. The thermal behaviors of both thin films and powders (cracked monoliths) were investigated using Raman, XRD, and N_2-sorption measurements to ensure a similar materials form by both methods.

The Raman spectra of the samples, calcined at 350 °C and annealed with 50 °C increments up to 550 °C, are shown in Figure 2. Up to 500 °C, the only phase observed is the $CoTiO_3$ phase, but above 500 °C, peaks related to the rutile phase of TiO_2 (at 267, 416, and 610 cm^{-1})[38] together with Co_3O_4 (peaks at 466, 508, and 670 cm^{-1})[39] also emerge and intensify with annealing time at 550 °C, compare Figure 2(e, f, and g).

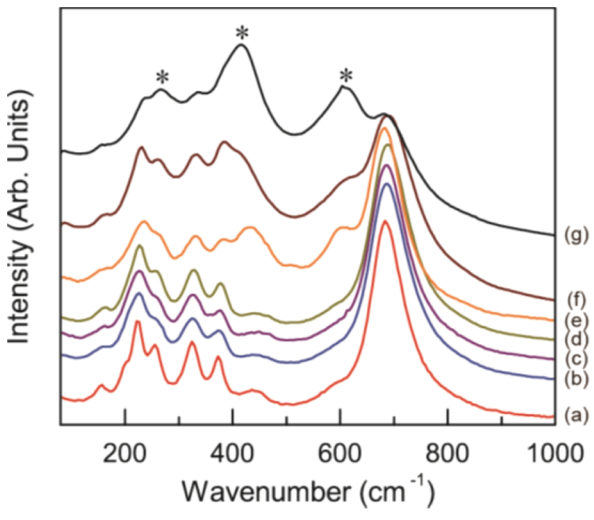

Figure 2. Temperature dependent Raman spectral changes of the mesoporous $CoTiO_3$. (a) 350 °C, (b) 400 °C, (c) 450 °C, (d) 500 °C, and (e, f, and g) 550 °C. * is rutile TiO_2.

Note also that the PXRD pattern of these samples also displays the rutile TiO_2 (ICDD PDF #00-021-1276) and Co_3O_4 (ICDD PDF #00-009-0418) related diffraction lines above 500 °C, see Figure S5. Therefore, it is reasonable to propose that the mesoporous $CoTiO_3$ undergoes a phase separation into TiO_2 and Co_3O_4 over 500 °C.

The N_2-sorption isotherms were also collected using both thin films (which require multiple coating and scraping of the films from hundreds of glass slides) and samples from spray coating to further prove the above proposal and to elucidate the nature of the pores. Both samples, collected from the thin films and spray coated films, show very similar N_2 sorption isotherms. Therefore, most of the data was collected using the spray coated samples, which are easier to prepare on a large scale. The N_2 sorption data display type IV isotherms at all temperatures, characteristic of mesoporous materials, with a record high surface area (around 316 m^2/g) and smaller pore size (3.1 nm) and pore volume (0.26 cm^3/g) at 350 °C. Figure 3(a) shows a set of N_2 sorption isotherms of mesoporous

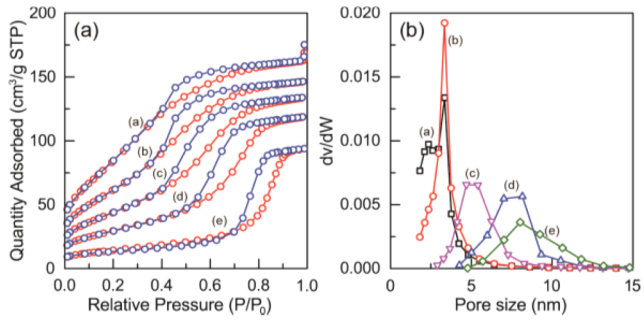

Figure 3. (a) N_2 sorption isotherms (red adsorption and blue desorption branches) and (b) the pore size distribution plots of the same sample of $CoTiO_3$.

$CoTiO_3$ annealed at different temperatures. The samples have two pore systems at low temperature (350 to 450 °C) and merge into one pore, while the pores increase in size with an increasing annealing temperature, Figure 3(b). The pores are quite narrow and uniform but gradually increase from 3.1 to 8.7 nm with increasing the annealing temperature from 350 to 550 °C, respectively. As an expense, the large surface area is lost during annealing steps (surface area drops from 316 to 52 m^2/g), compare data in Table 1. Note also that the pore size expansion is gradual with increasing annealing temperature.

We also collected a series of TEM images of the samples and observed that the images also accord with the Raman, XRD, and N_2 sorption data. The images display a sponge-like L_3 phase of mesoporous materials[40] (see Figure S6(a, b, and c), but, at 550 °C, one can also observe highly crystalline 20−30 nm nanoparticles in the samples, Figure S6(d). However, the sample annealed at 550 °C still provides type IV isotherm. These observations clearly indicate that the mesoporous $CoTiO_3$ is stable up to 500 °C and undergoes phase separation into rutile TiO_2 and Co_3O_4 nanocrystallites at around 550 °C.

Mesoporous $MnTiO_3$ Thin Films and Powders. We also investigated the Mn(II) system and found very similar behaviors to the Co(II) system. We have investigated 2−7 Mn(II) to 7 Ti(IV) and also 4 Mn(II) to 4 Ti(IV) mole ratios per $C_{12}EO_{10}$. The CTAB content of the sample was kept constant, at 1:1 CTAB:$C_{12}EO_{10}$ throughout the investigation. Figure S7(a) displays a series of FTIR spectra of the fresh samples with different Mn(II)/Ti(IV) mol ratio. The spectra

dx.doi.org/10.1021/cm503020y | Chem. Mater. 2014, 26, 6050−6057

Table 1. N_2 Sorption, Raman, and XRD Related Data of Mesoporous $CoTiO_3$, $MnTiO_3$, and $Li_4Ti_5O_{12}$

$CoTiO_3$				
temp (°C)	surface area (m^2/g)	pore size (nm)	pore volume (cm^3/g)	phase
350	316	3.1	0.26	$CoTiO_3$
450	227	3.3	0.23	$CoTiO_3$
450	161	4.0	0.21	$CoTiO_3$
500	107	5.4	0.19	$CoTiO_3$
550	52	8.7	0.15	Co_3O_4/ TiO_2
$MnTiO_3$				
temp (°C)	surface area (m^2/g)	pore size (nm)	pore volume (cm^3/g)	phase
350	445	3.1	0.40	$MnTiO_3$
400	370	3.2	0.36	$MnTiO_3$
450	270	3.4	0.31	$MnTiO_3$
500	124	5.6	0.20	$MnTiO_3$
550	33	15.6	0.16	Mn_2O_3/ TiO_2
$Li_4Ti_5O_{i2}$				
temp (°C)	surface area (m^2/g)	pore size (nm)	pore volume (cm^3/g)	phase
350	193	4.3	0.25	$Li_4Ti_5O_{12}$
400	152	5.2	0.27	$Li_4Ti_5O_{12}$
450	75	7.3	0.19	$Li_4Ti_5O_{12}$
500	65	9.9	0.21	$Li_4Ti_5O_{12}$
550	21	22	0.17	$Li_xTi_yO_{(x/2+2y)}$

display peaks (at 1308, 1468, and 1564 cm^{-1}) due to the nitrate species, coordinated to both Mn(II) and titania surface sites, indicating that while titania is forming in the gel-phase, the Mn(II) species remains unreacted at RT. The calcined samples, containing less Mn(II), produced transparent $MnTiO_3$−TiO_2, Figure S7(b), and the 7 to 7 and 4 to 4 samples produced only $MnTiO_3$. At all compositions, the films are high quality and highly transparent with an increasing intensity of the brown color with and increasing Mn(II) content in the samples, see Figure S7(b). The films absorbed both UV and visible region of the electromagnetic spectrum, where the absorption tails in the near IR region, Figure S7(c). By plotting their Tauc curves using an indirect gap relationship, we also found the band gap of the films that have a Mn(II) dependence; the band gap decreases from 1.92 to 1.77 to 1.63 and to 1.48 eV going from Mn(II)/$C_{12}EO_{10}$ mole ratios of 2 to 3 to 4 to 5 at 450 °C, respectively, see Figure S7(d). This trend shows that the $MnTiO_3$ domains are growing in a titania matrix with an increasing Mn(II) content in the samples and accords with the model in Scheme 1. However, the main focus of this work was on the 4 Mn(II) and 4Ti(IV) samples to form a pure $MnTiO_3$ phase.

The spray coating method was also optimized for the Mn(II) system to be able collect enough samples for the PXRD and N_2-sorption measurements. The XRD pattern displays very broad and week features that can be related to the ilmenite phase of the $MnTiO_3$ (ICDD PDF #00-002-0846) and the Mn_2O_3 (ICDD PDF #00-010-0069) and TiO_2 related diffraction line starts emerging upon annealing the samples above 500 °C and dominates the PXRD pattern at higher temperatures, Figure S8. Due to strong X-ray absorption and emission of the samples, the XRD patterns are too week to elucidate the structural details. However, Raman spectroscopy is a powerful technique and display peaks due to the phase separation related changes at around 500 °C. The spectra clearly display characteristic $MnTiO_3$ peaks,[41] at 158, 206, 224, 255, 326, 352, 426, 606, and 676 cm^{-1}, between 350 and 500 °C, indicating a nanocrystalline nature of the pore wall content, Figure S9. However, at higher temperatures the phase segregation species are also visible in both the PXRD patterns and Raman spectra; see Figures S8 and S9, respectively. These two techniques collectively provide information about the crystallinity of the pore-walls.

We also collected N_2 sorption data starting from 350 up to 550 °C using the same samples. The isotherms are type IV and characteristic of mesoporous materials, Figure S10(a). The surface area gradually decreases and the pore size increases with an increasing annealing temperature, see Figure S10 and Table 1 for the details. Similar to $CoTiO_3$, the mesoporous $MnTiO_3$ also collapse at around 500 °C and produce nanocrystalline Mn_2O_3−TiO_2 phases. However, these materials are still very important for many applications, because it is a homogeneous assembly of Mn_2O_3−TiO_2 nanoparticles in the form of thin films or monoliths.

The samples were further analyzed using TEM measurements. The thin films were ground into fine particles that look alike and show sponge-like pore-systems, see Figure 4. The images show that the pores are uniform and homogeneous throughout the films. Since the pores are randomly organized, it is difficult to identify the pore-wall and its crystallinity from the TEM images.

Mesoporous $Li_4Ti_5O_{12}$ Thin Films and Powders. The interest in mesoporous $Li_4Ti_5O_{12}$ as an anode material for the Li^+ ion batteries has grown immensely over the past few years.[16,28−32] However, the current synthetic methods produce powders with relatively smaller surface areas and with much thicker pore-walls. Although, the wall thickness is usually near the diffusion limits of Li^+ ions (typically around 10 nm), it is important to reduce it further to effectively charge and discharge these materials. One way to increase surface area and reduce the wall thickness is to produce $Li_4Ti_5O_{12}$ using smaller surfactant molecules. So far the most commonly investigated surfactant, used to synthesize mesoporous $Li_4Ti_5O_{12}$, is KLE (Karaton-liquid-*b*-poly(ethylene oxide, M_w of around 80000), which is a large copolymer and easy to assemble. Assembling the salt and polymerizing titania source with smaller surfactants is more difficult, especially for nonpolymerizing salts at room temperature, such as lithium salts. However, the MASA approach provides an effective solution to this problem, and the production of mesoporous $Li_4Ti_5O_{12}$ with a larger surface area and thinner pore-walls and adjustable pore size is possible using CTAB and $C_{12}EO_{1O}$ surfactant couples. We also know that many lithium salts can be self-assembled into lyotropic liquid crystalline mesophases with nonionic surfactants.[9] A broad range of $LiNO_3$ and TTB was used in this investigation, and the conditions required for a stoichiometric Li(I)/Ti(IV) ratio of 4/5 have been established. Note that these ratios are also the Li/$C_{12}EO_{10}$ and Ti/$C_{12}EO_{10}$ mole ratios. The optimization for both spin coating (for thin films) and spray coating (thicker and large quantity samples) has been performed by using FT-IR, Raman, XRD, and N_2-sorption experiments and is similar to $CoTiO_3$ and $MnTiO_3$; therefore, we will not discuss the steps again.

The samples, prepared using spray coating, were analyzed using PXRD, N_2-sorption, and Raman spectroscopy techniques to elucidate the temperature dependent behavior of the samples. The freshly prepared spray coated samples were first

dx.doi.org/10.1021/cm503020y | *Chem. Mater.* 2014, 26, 6050−6057

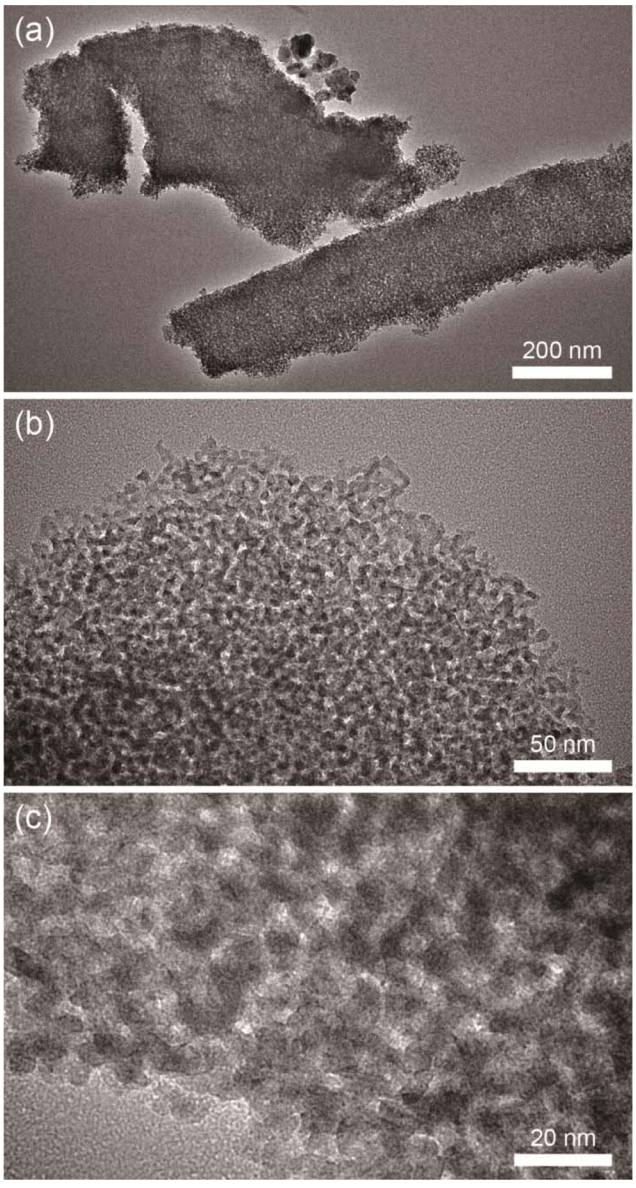

Figure 4. TEM images of mesoporous $MnTiO_3$, calcined at 450 °C, with different magnifications, the scale bars are (a) 200 nm, (b) 50 nm, and (c) 20 nm.

fast calcined at 350 °C and then scraped from the glass surface collected around 100−150 mg of powder for the N_2 sorption experiment. The same sample was used for the PXRD measurements and then further annealed at higher temperatures to simultaneously collect both N_2-sorption isotherms and PXRD patterns. The annealing steps were carried out by 50 °C increments. Figure 5 shows a series of N_2-sorption and PXRD patterns from those samples. All the isotherms are type IV, clearly indicating that the samples are mesoporous. Similar to mesoporous $CoTiO_3$ and $MnTiO_3$, the $Li_4Ti_5O_{12}$ also expands in pore size, while the surface area decreases with an increasing annealing temperature; see Figure 5 and Table 1 for the details. The pore size expansion with the annealing temperature is very gradual and uniform. Pore size is highly uniform at low temperatures, but with an increasing annealing temperature, the pore size distribution becomes highly nonuniform. The pore size can be tuned from 4.3 to 9.9 nm.

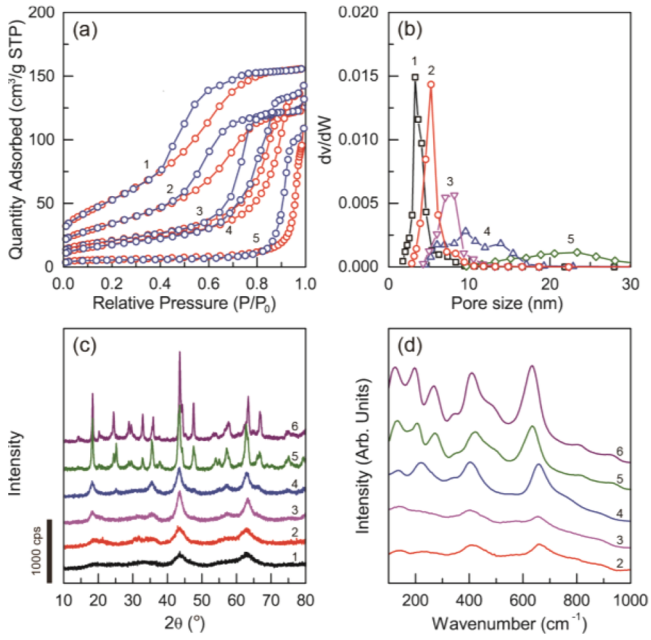

Figure 5. Changes in the mesoporous $Li_4Ti_5O_{12}$ with increasing annealing temperatures in the (a) N_2 sorption isotherms (at 1) 350, 2) 400, 3) 450, 4) 500, and 5) 550 °C), (b) pore size distribution plots (left to right, evaluated from the data in panel (a)), (c) PXRD patterns, and (d) Raman spectra, (the annealing temperatures are 1) 350, 2) 400, 3) 450, 4) 500, 5) 550, and 6) 600 °C).

The surface area also gradually drops with an increasing annealing temperature, see Table 1.

The PXRD patterns display very broad diffraction lines, corresponding to a pure spinel $Li_4Ti_5O_{12}$ phase (ICDD PDF #00-049-0207) even at 350 °C. The diffraction lines get more intense and sharpen slightly but remain almost the same with a similar fwhm up to 550 °C, and at around 550 °C a phase separation takes place and relatively larger $Li_4Ti_5O_{12}$ nanocrystallites and an unknown $Li_xTi_yO_{2y+x/2}$ phase form. Up to 500 °C, the pore-walls are nanocrystalline with a wall thickness of a few nanometers. Remember, these samples were annealed stepwise by 50 °C increments. One can also calcine the films or spray coated samples at higher temperature (between 350 and 550 °C). The samples heated straight at 550 °C, for example, differ from that of the samples annealed stepwise starting from 350 °C. The samples, heated straight at 550 °C, are still mesoporous with a relatively smaller pore size (4.7 nm and becomes 9.3 nm after 2 h annealing, compared with stepwise annealed sample 22 nm) and have larger surface area (63 m^2/g compared to 21 m^2/g), see Figure S11(a). These samples still diffract broadly, indicating nanocrystalline pore-walls. Moreover, the PXRD lines are much stronger, and the two samples are shown in Figure S11(c). However, at 550 °C, these samples also undergo phase separation; the phase separation is enhanced with increasing time, Figure S11(c). However, the samples calcined at higher temperature are more stable and resist high temperatures. The phase separation at 550 °C leads to an anatase phase of TiO_2 with larger, dominant $Li_4Ti_5O_{12}$ particles. Not only are the samples calcined at higher temperatures more stable but also the phase separation also proceeds differently and yields different products; compare the PXRD patterns in Figures 5(c) and S12. The elucidation of these mechanistic differences requires further study, and it is outside the scope of this investigation.

dx.doi.org/10.1021/cm503020y | *Chem. Mater.* 2014, 26, 6050−6057

The annealing process was monitored using Raman spectroscopy, Figure 5(d). The $Li_4Ti_5O_{12}$ related peaks[42,43] appear at as low as 350 °C and intensify by the increasing annealing temperature, and the new peaks start emerging at around 550 °C. The peak at 658 cm^{-1} completely shifts to 633 cm^{-1}; and a new shoulder appears at 480 cm^{-1}, and the peak, at 221 cm^{-1}, shifts or splits into two new peaks at 197 and 272 cm^{-1}. Two new peaks, at 809 and 922 cm^{-1}, appear and intensify by annealing at higher temperatures and are characteristic of surface peroxy species. These observations are consistent with the changes observed in the PXRD patterns. The origin of these changes is attributed to the crystallization of $Li_4Ti_5O_{12}$ and the phase change/separation at higher temperatures. The phase separation leads a new unidentified $Li_xTi_yO_z$, because the new peaks do not belong to any phase of pure titania.

We also analyzed these samples using TEM imaging. A set of TEM images of a sample annealed at 450 and 550 °C is shown in Figure 6. The TEM images clearly show that the samples have a uniform sponge-like porosity similar to the other two titanates. The flakes of the films are shown in Figure 6(a). Notice that these flakes are scraped from the glass substrate and ground for sometime. Both TEM and SEM images display uniform flakes, and no particles with a different morphology were observed in any of the samples. Figure 6(b) shows the TEM images of the same sample at higher magnifications. As seen in the images, the film particles are sponge-like and highly porous with pore sizes similar to the ones evaluated from the N_2 sorption data. Careful analysis of Figure 6(b) indicates pore wall thickness of around 3−4 nm and pore size of 7−10 nm, which are similar to the results obtained from the PXRD (Scherer analysis) and N_2 sorption data (pore size distribution plots). Figure 6(c) is a TEM image of a sample calcined straight at 550 °C. It displays a mesoporous structure with needle-like $Li_4Ti_5O_{12}$ nanocrystallites (5−10 wide by 10−20 nm long) around the pores, see Figure S13.

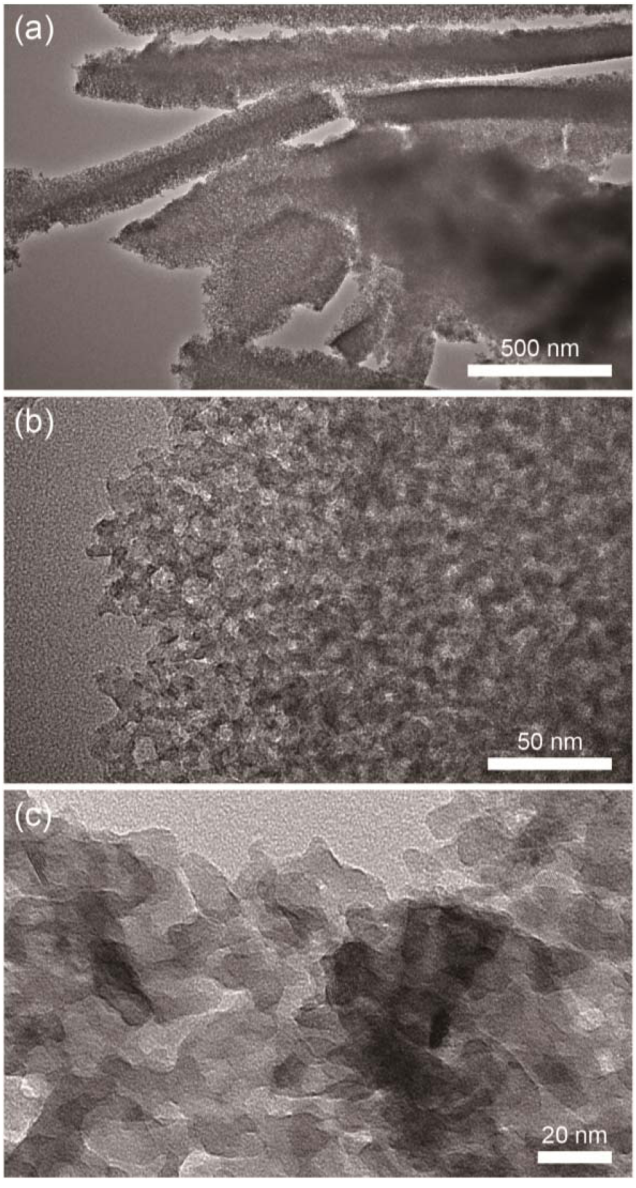

Figure 6. TEM images of mesoporous $Li_4Ti_5O_{12}$ thin films (a and b) annealed at 450 °C and (c) at 550 °C.

It is clear from the above data that the calcination temperature and annealing steps are critical obtaining well crystalline mesoporous $Li_4Ti_5O_{12}$. One of two different growth and separation mechanisms is effective, depending on the history of the samples. Definitely more stable walls can be formed if the samples are first calcined at high temperatures, and they show better resistance to high temperature annealing processes.

CONCLUSION

The molten salt assisted self-assembly method has been adopted to synthesize mesoporous thin films and powders of three new titanates ($CoTiO_3$, $MnTiO_3$, and $Li_4Ti_5O_{12}$). In this assembly process, a volatile solvent (ethanol) was used to homogeneously distribute all the ingredients and to allow for easy processing; spin or spray coatings are both possible. In the spin coating process, the spun solution immediately loses its volatile solvent and leaves behind salt (or hydrated salt) species that are in the liquid phase in the hydrophilic domains of the mesophase and which help the surfactants to assemble first into the LLC mesophase, then into a mesostructured semisolid with the condensation of the titania species over time. The spin or spray coated samples can be fast calcined straight at a desired temperature in 10−30 min. The fast calcination ensures complete burning of the surfactant species and the formation of metal titanates. All three examples investigated in this work are new in terms of pore structure, pore-wall composition, pore-wall thickness, and morphology as thin films as well as spongy porosity. Typical thickness of the films is around 400 nm, but it could be adjusted between a few tens and a few hundreds of nanometers by controlling the spin speed and ethanol content of the original solution. All titanates form at temperatures as low as 350 °C and are stable up to 500−550 °C. The pore walls of mesoporous $Li_4Ti_5O_{12}$ are nanocrystalline even at 350 °C and have thicker pore-walls with a smaller surface area. Simply, the low temperature crystallization results in a thicker pore-wall and smaller surface area in the $Li_4Ti_5O_{12}$ compared to $CoTiO_3$ and $MnTiO_3$. This behavior is also evident in the samples heated at higher temperatures, such that the titanate domains grow in size and eventually undergo phase separation at higher temperatures and display smaller surface area. Moreover with annealing, the step by step or calcining at higher temperatures, one can produce larger pores with a better pore wall crystallinity at the expense of losing their surface area. In all three systems, the surface area, obtained from metal titanates, reaches a record high, as high as 445 m^2/g. Surface

dx.doi.org/10.1021/cm503020y | Chem. Mater. 2014, 26, 6050−6057

area, pore-wall composition, pore-wall crystallinity, pore size, and pore volume can be adjusted by playing with the composition of the MASA ingredients and the annealing temperature. The MASA process is not limited to only these titanates; other binary, ternary, and also doping of titanates with different metal ions are also possible using this assembly process.

■ ASSOCIATED CONTENT

Supporting Information

Additional spectra (UV−vis, Raman, FTIR), diffraction patterns, N2 sorption, TEM, and SEM images for all three sets of samples. This material is available free of charge via the Internet at http://pubs.acs.org.

■ AUTHOR INFORMATION

Corresponding Author

*E-mail: dag@fen.bilkent.edu.tr.

Author Contributions

The manuscript was written through contributions of all authors. All authors have given approval to the final version of the manuscript.

Funding

TÜBİTAK 113Z730.

Notes

The authors declare no competing financial interest.

■ ACKNOWLEDGMENTS

The authors thank TÜBİTAK under project number 113Z730 for financial support. Ö.D. is a member of the Science Academy, Istanbul, Turkey.

■ ABBREVIATIONS

MASA, molten salt assisted self-assembly; TTB, titaniumtetrabutoixde; LLC, lyotropic liquid crystal

■ REFERENCES

(1) Albayrak, C.; Özkan, N.; Dag, Ö. *Langmuir* **2011**, *27*, 870.
(2) Karakaya, C.; Türker, Y.; Albayrak, C.; Dag, Ö. *Chem. Mater.* **2011**, *23*, 3062.
(3) Karakaya, C.; Türker, Y.; Dag, Ö. *Adv. Funct. Mater.* **2013**, *23*, 4002.
(4) Çelik, Ö.; Dag, Ö. *Angew. Chem., Int. Ed.* **2001**, *40*, 3800.
(5) Albayrak, C.; Soylu, A. M.; Dag, Ö. *Langmuir* **2008**, *24*, 10592.
(6) Türker, Y.; Karakaya, C.; Dag, Ö. *Chem.—Eur. J.* **2012**, *18*, 3695.
(7) Yang, P.; Zhao, D.; Margolese, D. L.; Chmelka, B. F.; Stucky, G. D. *Nature* **1998**, *396*, 152.
(8) Grosso, D.; Illia, G. J. A. A.; Crepaldi, E. L.; Charleux, B.; Sanchez, C. *Adv. Funct. Mater.* **2003**, *13*, 37.
(9) Grosso, D.; Boissiere, C.; Smarsly, B.; Brezensinski, T.; Pinna, N.; Albouy, P. A.; Amenitsch, H.; Antonietti, M.; Sanchez, C. *Nat. Mater.* **2004**, *3*, 787.
(10) Kong, L.; Chen, H.; Hua, W.; Zhang, S.; Chen, J. *Chem. Commun.* **2008**, 4977.
(11) Lee, J.; Orilall, M. C.; Warren, S. C.; Kuperman, M.; Disalvo, F. J.; Wiesner, U. *Nat. Mater.* **2008**, *7*, 222.
(12) Li, G. S.; Zhang, D. Q.; Yu, J. C. *Environ. Sci. Technol.* **2009**, *43*, 7079.
(13) Fan, X.; Wang, Y.; Chen, X.; Gao, L.; Luo, W.; Yuan, Y.; Li, Z.; Yu, T.; Zhu, J.; Zou, Z. *Chem. Mater.* **2010**, *22*, 1276.
(14) Jo, C.; Kim, Y.; Hwang, J.; Shim, J.; Chun, J.; Lee, J. *Chem. Mater.* **2014**, *26*, 3508.
(15) Qu, Y.; Zhou, W.; Fu, H. *ChemCatChem* **2014**, *6*, 265.
(16) Kang, E.; Jung, Y. S.; Kim, G.-H.; Chun, J.; Weisner, U.; Dillon, A. C.; Kim, J. K.; Lee, J. *Adv. Funct. Mater.* **2011**, *21*, 4349.
(17) Gu, D.; Schüth, F. *Chem. Soc. Rev.* **2014**, *43*, 313.
(18) Fattakhova-Rholfing, D.; Zaleska, A.; Bein, T. *Chem. Rev.* **2014**, DOI: 10.1021/cr500201c.
(19) Ma, Z.; Yu, J.; Dai, S. *Adv. Mater.* **2010**, *22*, 261.
(20) Poyraz, A. S.; Kuo, C. H.; Biswas, S.; King'ondu, C. K.; Suib, S. L. *Nat. Commun.* **2013**, *4*, 2952.
(21) Song, J. Y.; Wang, Y. Y.; Wan, C. C. *J. Power Sources* **1999**, *77*, 183.
(22) Shimura, H.; Yoshio, M.; Hoshino, K.; Mukai, T.; Ohno, H.; Kato, T. *J. Am. Chem. Soc.* **2008**, *130*, 1759.
(23) Kerr, R. L.; Miller, S. A.; Shoemaker, R. K.; Elliott, B. J.; Gin, D. L. *J. Am. Chem. Soc.* **2009**, *131*, 15972.
(24) Judeinstein, P.; Roussel, F. *Adv. Mater.* **2005**, *17*, 723.
(25) Poizot, P.; Laruelle, S.; Grugeon, S.; Dupont, L.; Tarascon, J.-M. *Nature* **2000**, *407*, 496.
(26) Ren, Y.; Armstrong, R.; Jiao, F.; Bruce, P. G. *J. Am. Chem. Soc.* **2010**, *132*, 996.
(27) Choi, N.-S.; Chen, Z.; Freunberger, S. A.; Ji, X.; Sun, Y.-K.; Amine, K.; Yushin, G.; Nazar, L. F.; Chao, J.; Bruce, P. G. *Angew. Chem., Int. Ed.* **2012**, *51*, 9994.
(28) Ye, Y.; Jo, C.; Jeong, I.; Lee, J. *Nanoscale* **2013**, *5*, 4584.
(29) Lee, J.; Jung, Y. S.; Warren, S. C.; Kamperman, M.; Oh, S. M.; Disalvo, F. J.; Wiesner, U. *Macromol. Chem. Phys.* **2011**, *212*, 383.
(30) Haetge, J.; Hartmann, P.; Brezensinski, K.; Janek, J.; Brezensinski, T. *Chem. Mater.* **2011**, *23*, 4384.
(31) Feckl, J. M.; Fominykh, K.; Döblinger, M.; Fattakhova-Rohlfing, D.; Bein, T. *Angew. Chem., Int. Ed.* **2012**, *51*, 7459.
(32) Yu, L.; Wea, H. B.; Lau, X. W. D. *Adv. Mater.* **2013**, *25*, 2296.
(33) Lin, C.; Fan, X.; Xin, Y.; Cheng, F.; Lai, M. O.; Zhou, H.; Lu, L. *Nanoscale* **2014**, *6*, 6651.
(34) Zhao, Y.; Sun, J.; Chen, X.; Zhu, H.; Yang, W. *New J. Chem.* **2014**, *38*, 1173.
(35) Albayrak, C.; Cihaner, A.; Dag, Ö. *Chem. - Eur. J.* **2012**, *18*, 4190.
(36) Dag, Ö.; Alayoglu, S.; Uysal, I. *J. Phys. Chem. B* **2004**, *108*, 8439.
(37) Zhou, G.-W.; Lee, D. K.; Kim, Y. H.; Kim, C. W.; Kang, Y. S. *Bull. Korean Chem. Soc.* **2006**, *27*, 368.
(38) Tompsett, G. A.; Bowmaker, G. A.; Cooney, R. P.; Metson, J. B.; Rodgers, K. A.; Seakins, J. M. *J. Raman Spectrosc.* **1995**, *26*, 57.
(39) Hadjiev, V. G.; Iliev, M. N.; Vergilov, I. V. *J. Phys. C: Solid State Phys.* **1988**, *21*, L199.
(40) McGrath, K. M.; Dabbs, D. M.; Yao, N.; Aksay, I. A.; Gruner, S. M. *Science* **1997**, *277*, 552.
(41) Zhou, G. W.; Kang, Y. S. *Mater. Sci. Eng., C* **2004**, *24*, 71.
(42) Aldon, L.; Kubiak, P.; Womes, M.; Jumas, J. C.; Olivier-Fourcade, J.; Tirado, J. L.; Corredor, J. I.; Pérez Vicente, C. *Chem. Mater.* **2004**, *16*, 5721.
(43) Baddour-Hadjean, R.; Pereira, J. P. *Chem. Rev.* **2010**, *110*, 1278.